Cite this: DOI: 10.1039/x0xx00000x

Received 00th January 2012,
Accepted 00th January 2012

DOI: 10.1039/x0xx00000x

www.rsc.org/

Evaluation of semiconducting molecular thin films solution-processed via the photoprecursor approach: The case of hexyl-substituted thienoanthracenes

Cassandre Quinton,[a] Mitsuharu Suzuki,*[a] Yoshitaka Kaneshige,[a] Yuki Tatenaka,[ab] Chiho Katagiri,[c] Yuji Yamaguchi,[c] Daiki Kuzuhara,[a] Naoki Aratani,[a] Ken-ichi Nakayama,[cd] and Hiroko Yamada*[ad]

Organic electronic devices are expected to be easily scalable and highly cost-effective, presuming good solution processability of high-performance organic semiconductors. However, there are the cases where an organic compound with promising semiconducting properties lacks adequate processability and does not form well-performing thin films through conventional solution-based deposition techniques. The photoprecursor approach, in which a soluble photoprecursor is solution-deposited on a substrate then converted to a target material by in-situ photoreaction, can be an effective means to evade such a problem. Herein, we describe a comparative evaluation of thin films deposited by three different methods; i.e., vacuum deposition, photoprecursor approach, and direct spin coating. Two highly crystalline molecular semiconductors, hexyl-substituted anthra[1,2-*b*:4,3-*b*':5,6-*b*'':8,7-*b*''']tetrathiophene (**C_6-ATT**) and anthra[1,2-*b*:5,6-*b*']dithiophene (or bent anthradithiophene, **C_6-BADT**), are employed in this study along with the corresponding newly synthesized α-diketone-type photoprecursors. In the case of **C_6-ATT**, thin films prepared through the photoprecursor approach are as good as those obtained by vacuum deposition in terms of surface smoothness and space-charge-limited-current (SCLC) mobility, while direct spin coating affords highly inhomogeneous films. For **C_6-BADT**, on the other hand, employment of the photoprecursor approach is not as effective, albeit it is still advantageous as compared to direct spin coating. These results highlight the power and limitations of the photoprecursor approach, and will serve as a basis for the preparation of practically useful organic devices through this unique approach.

1. Introduction

Solution processability is an important consideration in designing organic semiconductors, as facile and large-scale preparation of high-quality active layers is the key to achieving cost-effective organic devices.[1–8] However, some molecular compounds with promising semiconducting properties are not well compatible with conventional direct solution deposition, typically because of too strong self-interactions. Such interactions often lead to undesirable formation of large aggregates, or even complete insolubility in customary solvents for intended solution-deposition processes. Unsubstituted acenes[9] and tetrabenzoporphyrin[10–14] represent this class of compounds, and their use in solution-processed devices has been largely limited owing to the lack of general approach to obtain smooth, homogeneous films that can be favourably used in, for example, organic solar cells or light-emitting diodes.[15]

The precursor approach, in which a well-soluble precursor compound is solution-deposited then converted in situ to a target semiconductor, has been proposed to evade the above-mentioned obstacle. Among various types of precursor compounds, α-diketone-type photoprecursors of acenes are characterized by the extremely mild reaction conditions for their post-deposit conversion, where only visible-light irradiation is required.[16] Several α-diketone-type precursors have been employed in preparation of organic field-effect transistors and photovoltaic cells comprising hardly soluble acene compounds.[17–21] In the case of pentacene and 2,6-di(2-thienyl)anthracene, this approach can afford high-quality semiconducting thin films that are comparable to the corresponding vacuum-deposited films in terms of charge-carrier mobility.[19,21]

Meanwhile, to our knowledge, there is not yet a report on direct comparison between the photoprecursor approach and conventional solution processes. Such a comparison will answer the question of whether the photoprecursor approach is merely a means to enable indirect solution deposition of insoluble materials, or holds any substantial difference from the direct solution deposition regarding the quality of resulting thin films. With these in mind, we have prepared α-diketone-type

photoprecursors of two known soluble p-type semiconductors, tetrahexylanthra[1,2-*b*:4,3-*b*′:5,6-*b*″:8,7-*b*‴]tetrathiophene (**C_6-ATT**) and dihexylanthra[1,2-*b*:5,6-*b*′]dithiophene (**C_6-BADT**) (Fig. 1). Derivatives of **ATT** and **BADT** have been the subject of interest in several studies on charge-carrier transport characteristics.[22–28] These thieno-annulated anthracene systems have also been examined as building units of polymeric semiconductors.[27,29]

In the following sections, we describe the synthesis and reactivity of the α-diketone-type photoprecursors of **C_6-ATT** and **C_6-BADT** (compounds **1** and **2**, respectively), as well as the difference between the thin films deposited through vacuum deposition, photoprecursor approach, or direct spin coating. It is shown that, in the case of **C_6-ATT**, the photoprecursor approach can provide thin films whose structural and (opto)electronic characteristics are similar to those of the vacuum deposited counterparts, while direct spin coating affords considerably lower quality films having large grains and cracks. The other compound, **C_6-BADT**, is indicated to have stronger self-interactions as compared to **C_6-ATT**, and employment of the photoprecursor approach is not sufficient to obtain smooth films under the examined conditions. Nevertheless, the **C_6-BADT** films prepared by the photoprecursor approach are still of higher quality than the directly spin-coated samples when the same solvent system and spin-coating conditions are employed.

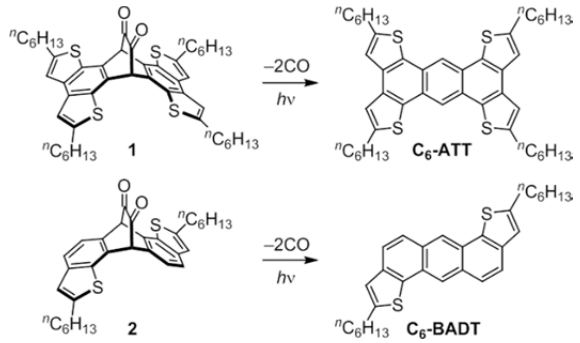

Fig. 1 Structures of **C_6-ATT**, **C_6-BADT**, and their α-diketone-type photoprecursors **1** and **2**.

2. Results and discussion

2.1. Synthesis

The synthetic pathway to photoprecursor **1** is outlined in Fig. 2. **C_6-ATT** was synthesized by the known oxidation of tetrathienylbenzene **3** with iron(III) chloride,[25,30] employing slightly modified conditions from the reported ones to obtain an improve yield of 86%. **C_6-ATT** is well soluble in common organic solvents (e.g., >10 mg mL^{-1} in chloroform), allowing straightforward purification by column chromatography. The Diels–Alder reaction of **C_6-ATT** with vinylene carbonate was conducted by heating at 180 °C in an autoclave for 3 days to

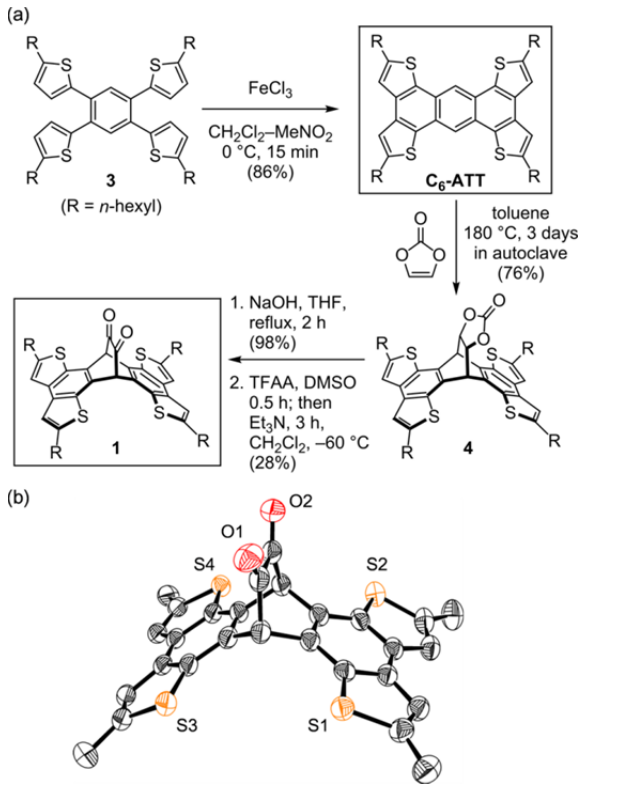

Fig. 2 (a) Synthetic route to α-diketone-type photoprecursor **1** through **C_6-ATT**. (b) Thermal ellipsoid representation of compound **1** in the single-crystalline state. Ellipsoids are at 50% probability. For clarity, only the first carbon atom is shown for each hexyl substituent, and the hydrogen atoms are omitted.

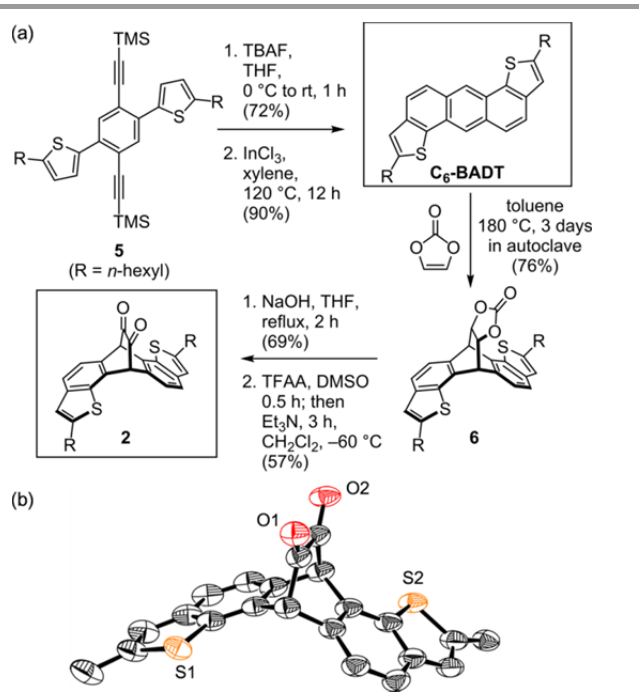

Fig. 3 (a) Synthetic route to α-diketone-type precursor **2** through **C_6-BADT**. (b) Thermal ellipsoid representation of compound **2** in the single-crystalline state. Ellipsoids are at 50% probability. For clarity, only the first carbon atom is shown for each hexyl substituent, and hydrogen atoms are omitted.

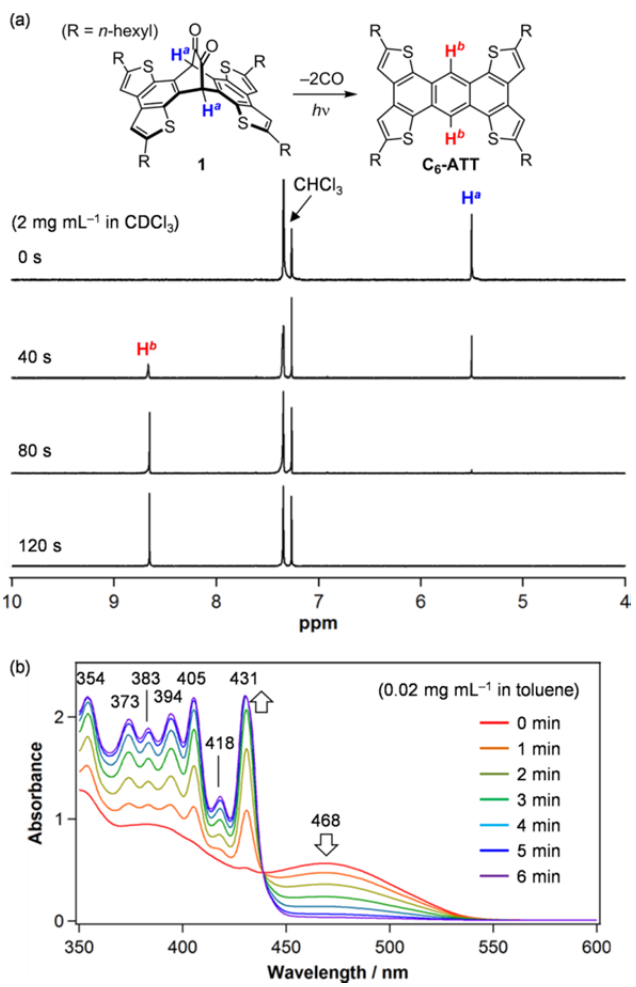

Fig. 4 Change in (a) NMR and (b) UV–vis absorption during the conversion of **1** to **C_6-ATT** under photoirradiation. The NMR spectra were taken in $CDCl_3$, while UV–vis spectra were measured in toluene. See ESI† for experimental details.

afford carbonate **4** in 76% yield. Compound **4** was hydrolyzed under basic conditions in 98% yield, and then subjected to Swern oxidation to afford the target α-diketone **1** as a yellow powder in an isolation yield of 28% after purification by silica gel chromatography and recrystallization.

The synthesis of photoprecursor **2** was performed as summarized in Fig. 3. The indium-catalyzed cyclization developed by Fürstner et al.[31] afforded **C_6-BADT** in 90% yield, which is as soluble as **C_6-ATT**. This protocol gave higher yields and reproducibility in our hands, and allowed easier scale up compared to the known photochemical reaction employed in the cyclization of 2,5-bis(2-thienyl)-1,4-divinylbenzene.[27] Similarly to compound **1**, the target α-diketone-type photoprecursor **2** was synthesized from **C_6-BADT** via the Diels–Alder addition with vinylene carbonate, hydrolysis under basic conditions, and Swern oxidation using trifluoroacetic anhydride (TFAA) as activator of dimethyl sulfoxide (DMSO). After purification by silica gel column chromatography and recrystallization, compound **2** was isolated as a yellow powder in 57% yield.

Hence, the syntheses of new photoprecursors **1** and **2** were completed in few steps from the corresponding thienoanthracenes **C_6-ATT** and **C_6-BADT**, respectively. The final products and intermediates were unambiguously identified by ^{1}H and ^{13}C NMR, and mass spectroscopic measurements. In addition, the structures of **1** and **2** were confirmed by single-crystal X-ray analysis as shown in Figs. 2b and 3b (see also Fig S6 in ESI†). **C_6-ATT**, **C_6-BADT**, compounds **1** and **2** were all purified by recrystallization, and their purities were checked to be >99% by high-performance liquid chromatography prior to use in the preparation of thin films.

2.2. Photoreactivity

α-Diketone-type photoprecursors **1** and **2** are smoothly converted to the corresponding anthracene derivatives **C_6-ATT** and **C_6-BADT**, respectively, upon photoirradiation in solution. The quantitative one-to-one conversion was confirmed by monitoring the reactions with NMR and UV–vis absorption spectroscopy. As shown in Fig. 4a, precursor **1** in $CDCl_3$ shows a ^{1}H NMR peak at 5.50 ppm corresponding to the bridgehead protons (H^a), which decreases and eventually disappears over the curse of the photoreaction. Concomitantly, a peak emerges at 8.67 ppm, which can be ascribed to the anthracene protons (H^b) of **C_6-ATT**. The reaction completed without formation of any detectable side products in these measurements. The change in photoabsorption is associated with a clear isosbestic point at 439 nm (Fig. 4b), indicating the constant reaction stoichiometry and the absence of a secondary reaction. The quantitative conversion of **2** was also shown by the same experiments (Fig. S1 in ESI†).

The reaction quantum yields (Φ_r) were determined based on the change in UV–vis absorption at the initial stage of each photoreaction (see the Experimental section for the method). The results show that increased thieno-annulation leads to lower efficiency of the photoreaction; namely, the Φ_r values in toluene are 0.37 for the parent anthracene diketone (**ADK**), 0.25 for the doubly thieno-annulated derivative **2**, and 0.21 for the quadruply thieno-annulated derivative **1** (Table 1). At the same time, the Φ_r values of precursors **1** and **2** are still considerably higher than those of tetracene diketone (**TDK**, $\Phi_r \approx 0.1$) and pentacene diketone (**PDK**, $\Phi_r = 0.027$). Here, Φ_r

Table 1 Reaction quantum yields for the photo-induced decarbonylation of α-diketone-type photoprecursors in toluene.[a]

Photoprecursor	**1**	**2**	**ADK**	**TDK**	**PDK**
Φ_r	0.21	0.25	0.37	~0.10[b]	0.027

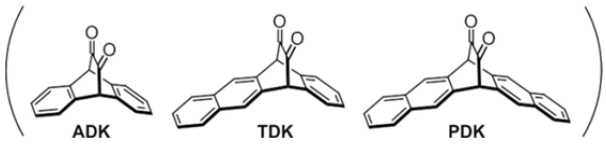

[a]Value for **ADK** was determined by the absolute method, and others were determined by the relative method. [b]Rough estimation because of significant overlap of absorption peaks between the reactant and product. Experimental details are described in the Experimental section.

rapidly decreases with linear extension of the acene framework from **ADK** to **TDK** and to **PDK**, while the nonlinear thieno-annulation from **ADK** to **1** and to **2** results in relatively minor decrease in Φ_r.

Based on the above observations, photoreaction in the solid state was expected not to be a problem for **1** and **2**, considering that **PDK**, which has a much lower Φ_r than **1** and **2**, can be photoconverted to pentacene both in the thin-film and single-crystalline states.[19,32] The solid-state conversion of precursors **1** and **2** to **C_6-ATT** and **C_6-BADT**, respectively, was monitored by IR spectroscopy as shown in Fig. 5. The carbonyl stretches of the α-diketone unit are observable around 1730 cm^{-1} for thin-film samples, which disappear upon irradiation of 470-nm light at 200 mW cm^{-2} for 30 min under a nitrogen atmosphere, indicating completion of the photo-induced decarbonylation in the films. Note that these conditions are the same as those employed for the photoconvertion of the α-diketone-type precursor of linear anthradithiophene,[18] while a longer reaction time is needed for **PDK**.[19]

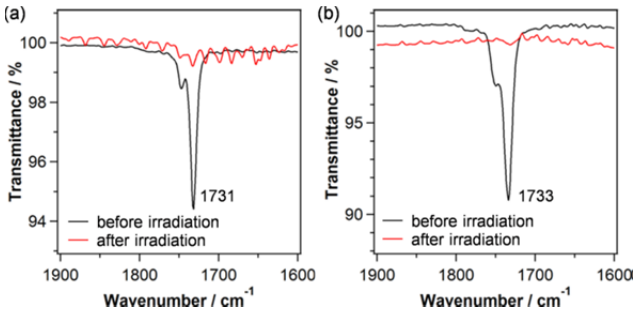

Fig. 5 Solid-state IR spectra before and after the photolysis: (a) α-diketone **1** to **C_6-ATT** (b) α-diketone **2** to **C_6-BADT**. The films were prepared by spin coating of a 3 mg mL^{-1} solution of **1** or **2** in chloroform. Irradiation conditions: 470 nm, 200 mW cm^{-2}, 30 min.

2.3. Optoelectronic properties of thin films

UV–vis absorption characteristics are essentially the same for the three differently prepared films in each case of **C_6-ATT** and **C_6-BADT**. Specifically, the absorption spectra of **C_6-ATT** films consist of five major peaks around 330, 344, 380, 411, and 437 nm associated with an absorption onset at 445 nm (2.79 eV) regardless of the deposition process (Fig. 6a). Similarly, **C_6-BADT** films show absorption peaks at about 295, 390, and 425 nm associated with an absorption onset around 445 nm with little variations among the three differently prepared samples (Fig. 6b).

Both compounds show redshift of the photoabsorption peaks in the solid state as compared to in solution. The degree of redshift is larger for **C_6-BADT**, the longest-wavelength absorption peak of which shifts by ca. 0.10 eV from 411 to 425 nm associated with considerable broadening of all the peaks. This indicates perturbation of molecular electronic structure in the thin films through nonspecific intermolecular interactions involving multiple modes and degrees. The corresponding redshift is smaller for **C_6-ATT**, being only 0.04 eV from 431 to 437 nm with relatively minor broadening of the peaks. Consequently, the absorption onset of **C_6-BADT** is essentially the same as that of **C_6-ATT** in the thin-film state. These observations indicate that **C_6-BADT** has somewhat stronger intermolecular interactions than **C_6-ATT** in the solid state. At the same time, no effective, specific intermolecular interaction that leads to the emergence of a new peak is indicated in these spectra even for **C_6-BADT**. This is in contrast to the case of pentacene deposited by the photoprecursor approach, which shows long-wavelength absorption and fluorescent peaks that can be attributed to the formation of π-stacks in the solid state.[33]

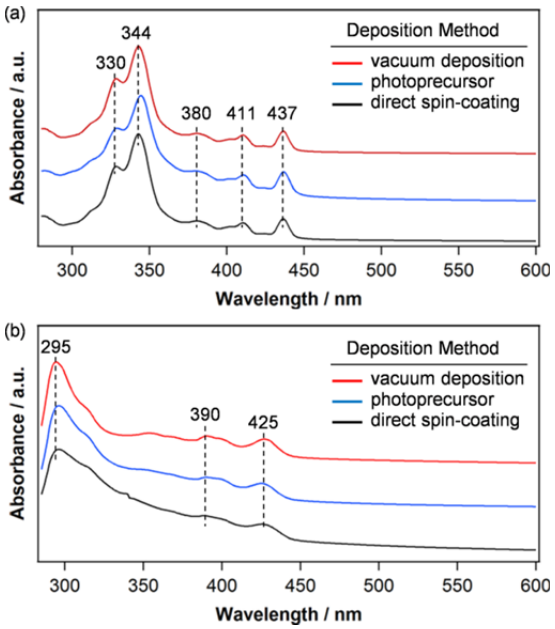

Fig. 6 UV–vis absorption spectra of thin films deposited by the three different methods: (a) **C_6-ATT** (b) **C_6-BADT**.

Table 2 Optical band gap energies ($E_{g,opt}$) and estimated frontier-orbital energies of **C_6-ATT** and **C_6-BADT** in the thin-film state.

	Deposition method	$E_{g,opt}$ [eV][a]	HOMO [eV][b]	LUMO [eV][c]
C_6-ATT	vacuum deposition	2.79	–5.52	–2.73
	photoprecursor	2.79	–5.48	–2.69
	direct spin coating	2.79	–5.47	–2.68
C_6-BADT	vacuum deposition	2.81	–5.40	–2.59
	photoprecursor	2.79	–5.39	–2.60
	direct spin coating	2.79	–5.43	–2.64

[a]Calculated from the absorption onsets. [b]Estimated by photo-electron spectroscopy in air. [c]Calculated as HOMO + $E_{g,opt}$.

The highest occupied molecular orbital (HOMO) energies of **C_6-ATT** and **C_6-BADT** in the thin-film state were estimated by photo-electron spectroscopy (PES) in air.[34] Here again, the difference in deposition process does not lead to major changes; namely, the observed HOMO energies are from –5.52 to –5.47 eV for **C_6-ATT** and from –5.43 to –5.39 eV for **C_6-BADT**

(Table 2, and Figs. S2 and S3 in ESI†). The HOMO levels were also estimated from the onset of the first oxidation potential (E^{ox}_{onset}) in cyclic voltammograms (CVs) according to the known empirical equation HOMO = $-E^{ox}_{onset}$ – 4.8 eV, where E^{ox}_{onset} is referenced to the ferrocene/ferrocenium standard.[35] The obtained values are –5.25 and –5.40 eV for **C_6-ATT** and **C_6-BADT**, respectively (Fig. S4 in ESI†). Thus, **C_6-BADT** has a lower HOMO level than **C_6-ATT** in solution according to the CVs, which parallels the results of density functional theory (DFT) calculations (Figs. S5 in ESI†). On the other hand, the PES measurements indicate that the HOMO level is higher for **C_6-BADT** in thin films. This discrepancy is assumed to be caused by the difference in intermolecular interactions in the condensed phase, as observed in the UV–vis spectra of the thin films. The LUMO levels were also estimated based on the equation LUMO = HOMO + $E_{g,opt}$, where $E_{g,opt}$ stands for the optical band gap obtained from the UV–vis absorption spectra of thin films. The values are summarized in Table 2.

2.4. Structural characteristics of thin films

Thin films of **C_6-ATT** and **C_6-BADT** were prepared on ITO/glass substrates with a MoO_3 buffer layer, which were also used for the space-charge-limited-current (SCLC) measurements described in the next section. Vacuum deposition was performed at a rate of 1.8 nm min^{-1} and a pressure of 1.2 × 10^{-4} Pa. Deposition by the photoprecursor approach was conducted by spin coating of a 10 mg ml^{-1} solution of photoprecursor **1** or **2** in chloroform at 800 rpm, followed by irradiation of 470-nm light at 200 mW cm^{-2} for 30 min in a nitrogen atomosphere. Direct solution deposition was first tried by spin coating of a 10 mg ml^{-1} solution of **C_6-ATT** or **C_6-BADT** in chloroform at 800 rpm as in the case of the photoprecursor approach; however, highly inhomogeneous films with visually observable cracks were obtained in these cases. The unfavourable morphology can be ascribed to the high tendency of **C_6-ATT** and **C_6-BADT** to aggregate from the chloroform solutions, and in turn, it is a clear manifestation of the power of photoprecursor approach to afford smoother films based on such materials. The quality of directly spin-coated films was improved when a 1:1 mixture of chloroform and chlorobenzene was used as solvent, so that the resulting films look homogeneous to the eye.

The microscopic surface morphology of the resulting films was investigated by tapping-mode atomic-force microscopy (AFM), and the crystallinity of the films was examined by out-of-plane X-ray diffraction (XRD) analysis. Fig. 7 shows the results for three differently prepared samples of **C_6-ATT**. The vacuum-deposited film has a relatively smooth surface with a root-mean square (RMS) roughness of 1.94 nm (Fig. 7a). It also has a moderate crystallinity showing a sharp diffraction peak at $2\theta = 4.62°$ (d = 19.1 Å) associated with a weak diffraction at 2θ = 9.25° (d = 9.56 Å) (Fig.7d). Although these peaks do not match with the diffraction pattern simulated from the single-crystal X-ray diffraction data (Table S3 in ESI†), the d-spacing calculated for the first diffraction is close to the lateral molecular dimension of **C_6-ATT** (~21 Å, Fig. S6a in ESI†), indicating an edge-on mode arrangement of molecules towards the substrate. The thin-film deposited via the photoprecursor approach has a smoother surface having an RMS value of 0.69 nm, and the difference between the highest and lowest points is only about 5 nm in the observed area (Fig 7b). The XRD pattern is similar to that of the vacuum deposited film, but with weaker peak intensities so that the second peak cannot be distinguish from the noise (Fig 7e).

The surface morphology of the film directly spin-coated from a chloroform–chlorobenzene (1:1) solution is significantly different from the two described above—the film contains large grains, whose lateral dimensions reach a few μm or even larger (Fig 7c). The height difference within the observed area is over 50 nm, which is similar to the average thickness of the film (ca. 50 nm). This high roughness prevents the film from being employed in the SCLC measurement, since the effective film thickness and interface area are hard to define. It would also be unfavourable to employ such a highly inhomogeneous film in electronic devices. The X-ray diffraction from the directly spin-coated film is significantly stronger as compared to the films prepared by vacuum deposition and photoprecursor approach (Fig 7d–f). This indicates that large crystalline domains are formed in the direct spin-coating conditions, which correlates well with the observation of significantly large domains by AFM.

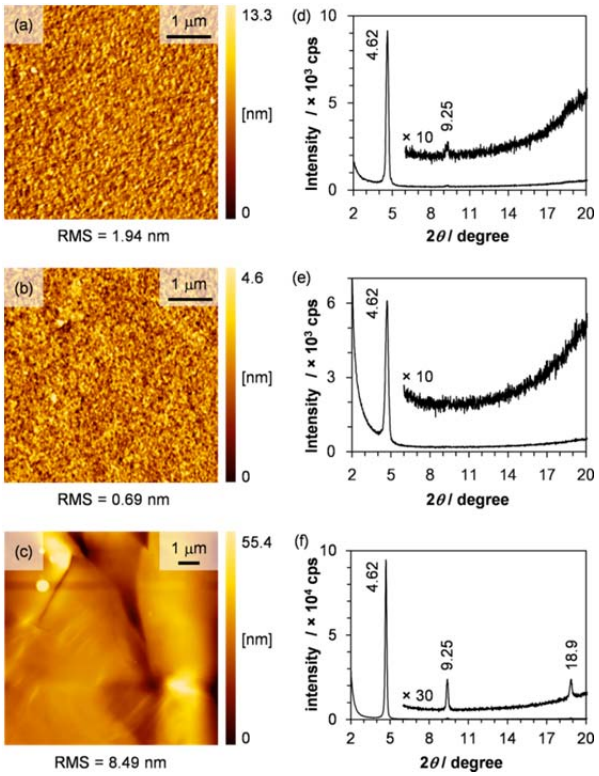

Fig. 7 AFM images (a–c) and out-of-plane XRD patterns (d–f) of thin films of **C_6-ATT**. Thin films are prepared by vacuum deposition (a, d), photoprecursor approach (b, e), or direct spin coating (c, f).

Fig. 8 summarizes the results for **C_6-BADT**. The vacuum-deposited film of **C_6-BADT** has larger grains compared to the

corresponding **C_6-ATT** film, indicating a higher tendency of the former compound to aggregate than the latter. This is consistent with the results of UV–vis and ionization potential measurements described earlier in Section 2.3. On the other hand, the surface roughness is similar for the two cases; specifically, the RMS values are 1.94 and 1.66 nm for the vacuum deposited **C_6-ATT** and **C_6-BADT**, respectively (Figs. 7a and 8a). The XRD measurement gave four distinct peaks at $2\theta = 4.91$, 9.90, 14.7, 19.8° corresponding to the *d*-spacings of 18.0, 8.93, 6.03, and 4.48 Å, respectively (Fig. 8d). The first peak is not very far from the (001) diffraction of the previously reported single-crystal structure ($c = 22.2$ Å), indicating an end-on-mode arrangement of molecules against the substrate.[27] The deviation of about 4 Å may be explained by a tilt of molecules in relation to the c^* axis in the thin-film state as compared to the α (90°) or β (91°) of the single-crystal unit cell, or difference in the orientation of alkyl chains.

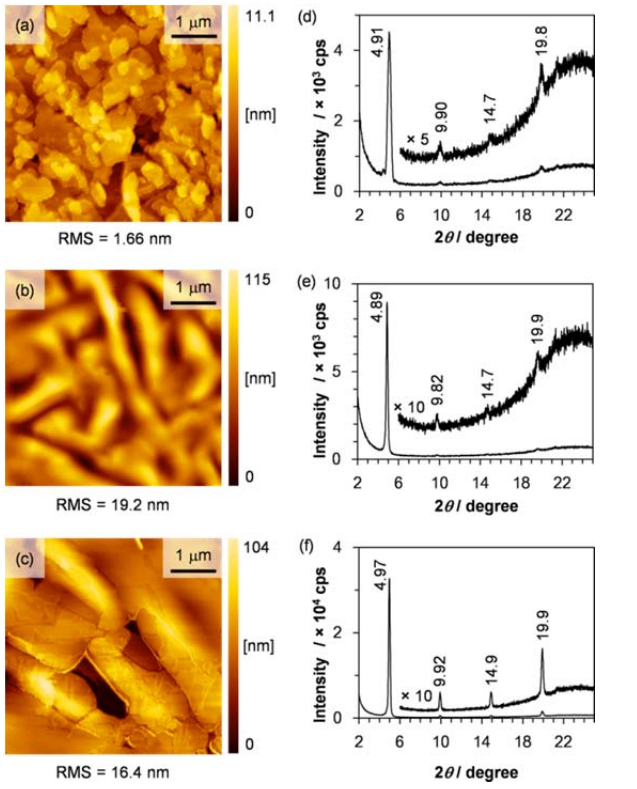

Fig. 8 AFM images (a–c) and out-of-plane XRD patterns (d–f) of thin films of **C_6-BADT**. The samples are prepared by vacuum deposition (a, d), photoprecursor approach (b, e), or direct spin coating (c, f).

The XRD pattern of the **C_6-BADT** film deposited by the photoprecursor approach is similar to that of the vacuum-deposited film, having a strong diffraction at $2\theta = 4.89°$ associated with weak diffractions at 9.82, 14.7, and 19.9°, although the third peak is hard to distinguish from the noise (Fig. 8e). On the other hand, the AFM images show different features between those two films; namely, the film prepared from the photoprecursor **2** has larger, but structurally less defined domains (Fig. 8b). The RMS value is as large as 19.2 nm, with the difference between the highest and lowest points exceeds 100 nm within the scanned area. Further investigation has revealed that the film deposited by the photoprecursor approach is similar to the directly spin-coated films in terms of surface roughness in the case of **C_6-BADT**. The RMS value for the directly spin-coated film is 16.4 nm, and the difference between the highest and lowest points is over 100 nm (Fig. 8c). On the other hand, the grain size is much larger for direct spin coating, probably because of the use of a higher boiling-point solvent (chlorobenzene) and thus slower growth of crystallites. In accordance with this, the intensity of X-ray diffraction is much stronger for the directly spin-coated film (Fig. 8f).

These results demonstrate the potential and limitations of the photoprecursor approach. It can be stated that the solution processability of highly crystalline materials is generally improved by employing the photoprecursor approach. This was manifested by the difference in the quality of **C_6-ATT** and **C_6-BADT** films when chloroform was employed as a solo solvent—direct spin coating led to cracked films whereas the films were visually homogeneous when deposited by the photoprecursor approach. Indeed, the film quality in terms of microscopic surface morphology and crystallinity is as high as the vacuum-deposited film in the case of **C_6-ATT**. For **C_6-BADT**, on the other hand, the quality of the thin film prepared by the photoprecursor approach is considerably lower than the vacuum-deposited sample. The intrinsic aggregation property of **C_6-BADT** seems to have a more profound effect than that of **C_6-ATT**, and hard to overcome just by employing the photoprecursor approach at least under the examined conditions.

2.5. Space-charge-limited-current measurements

The charge-carrier mobility in **C_6-ATT** deposited by the photoprecursor approach was measured by the SCLC technique. While the field-effect mobility probes the property of materials only at the interface with gate dielectrics, the SCLC method evaluate the bulk mobility, and thus would be more suitable when comparing bulk qualities of thin films.

Hole-only devices with the structure of [ITO/MoO_3/**C_6-ATT**/MoO_3/Al] were fabricated for the measurements. As shown in Fig. S7b of ESI†, a carrier mobility of 2.07×10^{-5} cm^2 V^{-1} s^{-1} was obtained when the active layer was deposited by the photoprecursor approach. This value is in the same range as that obtained for a vacuum deposited film (1.79×10^{-5} cm^2 V^{-1} s^{-1}, Fig. S7a in ESI†), which is reasonable considering that these two deposition methods afford thin films having similar crystallinity and morphology as described in Section 2.4. The directly spin-coated film of **C_6-ATT** is too rough to obtain a reliable mobility by the SCLC method, because its effective thickness is hard to define. For the same reason, SCLC mobilities were not measured for the solution-processed films of **C_6-BADT**.

3. Conclusions

We have synthesized new α-diketone-type photoprecursors **1** and **2**, and evaluated the thin films of **C_6-ATT** and **C_6-BADT**

deposited by the photoprecursor approach in comparison with those prepared by vacuum deposition and direct spin coating. The syntheses were completed in good overall yields from the known starting materials, and the target photoprecursors were unambiguously identified by spectroscopic analyses and single-crystal X-ray diffractometry. The comparative evaluation revealed that, in the cased of **C_6-ATT**, the photoprecursor approach provided thin films that have considerably higher quality than the directly spin-coated samples, and are comparable to the vacuum deposited counterparts in terms of surface morphology and SCLC mobility. In contrast, the photoprecursor approach had only limited success under the examined processing conditions in the case of **C_6-BADT**, which seemed to have a stronger tendency to self-aggregate in comparison with **C_6-ATT** according to the spectroscopic and microscopic analyses.

These results show that the photoprecursor approach is more than just a way to enable the use of solution-based techniques for deposition of insoluble (or hardly soluble) materials. Rather, this approach also extends the range of applicable solution-processing conditions for soluble semiconducting materials. As observed for **C_6-ATT**, the photoprecursor approach can afford thin films of much higher quality than direct solution deposition without extensive search for processing conditions. Even in the more difficult case of **C_6-BADT**, the film quality is higher for the photoprecursor method than direct spin coating when the same solvent (chloroform) was employed. It would be worth noting here that the α-diketone-type photoprecursors **1** and **2** are well soluble in common organic solvents and not strongly aggregating, so that their thin films are highly homogeneous without forming large grains in a wide variety of spin-coating conditions (different solvent systems, solution concentrations, spin rates, etc.) (Fig. S8 in ESI†). This considerably simplifies the optimization of solution-deposition conditions, and is highly advantageous especially when the choice of solvent is limited—a typical example is the solution processing of multi-layer thin films by employing orthogonal solvent systems. In addition, the photoprecursor approach allows us to control the film morphology through adjusting the photoreaction conditions including the light intensity and duration, or by the use of small amounts of solvent additives.[19] Further investigation along these lines is underway in our group.

4. Experimental

4.1. Synthesis and structural characterization of compounds

General. Anhydrous THF (Super Plus grade, stabilizer free), toluene (Super Plus grade), and CH_2Cl_2 (Super grade) were obtained from Kanto Chemical and used as received. Anhydrous DMSO (Super Dehydrated grade) was obtained from Wako Chemical, and used as received. *N*,*N*-diisopropylethylamine was distilled and stored over KOH. All the other solvents and chemicals were of reagent grade obtained commercially and used without further purification. Room temperature, or rt, means 20–25 °C. Thin layer chromatography and flash column chromatography were performed on Merck Silica Gel 60 F_{254} (Art. 5554) and Kanto Silica Gel 60N (spherical, 40–50 μm), respectively. ^{1}H NMR and ^{13}C{^{1}H} NMR spectra were recorded on a JEOL JNM-AL300 or a JNM-ECP400 spectrometer using tetramethylsilane or solvent resonances as internal standards. Mass spectra were recorded on a JEOL AccuTOF/JMS-T100LC (ESI), JEOL JMS-700 (EI), or Bruker Autoflex II (MALDI-TOF) instrument. Infrared spectra were recorded on a JASCO FT/IR-4200 spectrometer with an ATR PRO450-S attachment. Melting points were measured on a Stanford Research System OptiMelt MPA100 apparatus.

1,2,4,5-Tetrakis(5-hexylthiophen-2-yl)benzene (3). To a solution of 2-hexylthiophene (1.3 mL, 7.2 mmol, 6.4 equiv) in anhydrous THF (100 mL) under argon was added a solution of *n*-butyllithium (1.6 M in hexanes, 5.0 mL, 8.0 mmol, 7.1 equiv) at –78 °C. The mixture was stirred at the same temperature for 1 h, and a solution of $ZnCl_2$ (1.3 g, 9.5 mmol, 8.5 equiv) in THF (50 mL) was added to it. The mixture was stirred for 1 h at room temperature, to which a solution of 1,4-dibromo-2,5-diiodobenzene (0.55 g, 1.1 mmol) and $Pd(PPh_3)_4$ (29 mg, 25 μmol, 2.2 mol%) in THF (30 mL) was added. The mixture was further stirred at 80 °C for 12 hours, before cooled to room temperature and the solvent was removed under reduced pressure. The mixture was then partitioned between CH_2Cl_2 and sat. NH_4Cl. The organic layer was collected and the aqueous layer was extracted with CH_2Cl_2. The combined organic layers were dried over anhydrous Na_2SO_4, filtered, and evaporated. The resulting crude product was purified by flash silica gel column chromatography (hexanes) to give a pale yellow solid (0.60 g, 0.81 mmol, 72%). The product was identified by comparing its ^{1}H NMR spectrum with the literature data.[25] ^{1}H NMR (300 MHz, $CDCl_3$): δ 7.57 (s, 2H), 6.76 (d, J = 3.5 Hz, 4H), 6.64 (d, J = 3.7 Hz, 4H), 2.76 (t, J = 7.5 Hz, 8H), 1.66–1.61 (m, 8H), 1.38–1.26 (m, 24H), 0.88 (distorted t, J = 7.0 Hz, 12H).

2,5,9,12-Tetrahexylanthra[1,2-*b*:4,3-*b′*:5,6-*b″*:8,7-*b‴*]tetrathiophene (C_6-ATT). A solution of iron(III) chloride (0.60 g, 3.7 mmol, 8.1 equiv) in nitromethane (6 mL) was added dropwise to a solution of **3** (0.34 g, 0.46 mmol) in anhydrous CH_2Cl_2 (900 mL) at 0 °C. After 15 min, methanol (150 mL) was added and the mixture was stirred for 1 h. The product was collected by filtration and rinsed with methanol. The crude product was purified by flash silica gel column chromatography (hexanes/$CHCl_3$, 3:1) to give a yellow solid (0.29 g, 0.39 mmol, 86%). The product was identified by comparing its ^{1}H NMR spectrum with the literature data.[25] ^{1}H NMR (300 MHz, $CDCl_3$): δ 8.67 (s, 2H), 7.35 (s, 4H), 3.04 (distorted t, J = 7.5 Hz, 8H), 1.88–1.82 (m, 8H), 1.54–1.34 (m, 24H), 0.92 (t, J = 7.0 Hz, 12H).

2,5,9,12-Tetrahexyl-7,14,15,19-tetrahydro-7,14-[4,5]epidioxoloanthra[1,2-*b*:4,3-*b′*:5,6-*b″*:8,7-*b‴*]tetrathiophen-17-one (4). C_6-ATT (1.0 g, 1.4 mmol) and vinylene carbonate (8.0 mL, 13 mmol, 93 equiv) in anhydrous toluene

(50 mL) were put in an autoclave and stirred at 180 ºC for 3 days. The reaction mixture was cooled to room temperature and the solvent was evaporated, to which methanol was added. The product was isolated by filtration and further purified by flash silica gel column chromatography (hexanes; hexanes/$CHCl_3$, 2:1) to give a pale brown solid (0.86 g, 1.0 mmol, 76%). ^{1}H NMR (300 MHz, $CDCl_3$): δ 7.29 (s, 2H), 7.28 (s, 2H), 5.31–5.30 (m, 2H), 5.11–5.10 (m, 2H), 2.95 (m, *J* = 7.0 Hz, 8H), 1.78 (m, 8H), 1.43–1.25 (m, 24H), 0.90 (distorted t, *J* = 7.0 Hz, 12H); ^{13}C NMR (75 MHz, $CDCl_3$): δ 147.4, 146.8, 134.3, 134.2, 134.2, 133.3, 131.7, 127.4, 126.1, 119.7, 119.6, 76.5, 45.2, 31.6, 31.6, 31.4, 31.3, 31.1, 28.9, 28.8, 22.6, 14.1; HRMS (ESI): *m*/*z* calcd. for $C_{49}H_{60}O_3S_4$ ([M + Na]$^+$) 847.3323, found 847.3323; m.p.: 163 °C.

2,5,9,12-Tetrahexyl-7,14-dihydro-7,14-ethanoanthra[1,2-*b*:4,3-*b*′:5,6-*b*″:8,7-*b*‴]tetrathiophene-15,16-dione (1). To a solution of 4 M NaOH (10 mL) were added THF (10 mL) and the vinylene carbonate adduct **4** (0.66 g, 0.80 mmol) under a N_2 atmosphere. The mixture was stirred at reflux for 2 h. After cooling to room temperature, the mixture was acidified with 1 M HCl. After addition of water, the mixture was extracted with chloroform, and the combined organic layer was washed with water and brine, dried over Na_2SO_4, filtered, and evaporated. The resulting crude product was purified by flash silica gel column chromatography (hexanes/EtOAc, 3:1) to give the corresponding diol as a pale yellow solid (0.63 g, 0.79 mmol, 98%). ^{1}H NMR (300 MHz, $CDCl_3$): δ 7.29 (s, 2H), 7.28 (s, 2H), 5.08 (m, 2H), 4.31 (m, 2H), 2.98–2.93 (t, *J* = 7.5 Hz, 8H), 2.29 (m, 2H), 1.81–1.77 (m, 8H), 1.42–1.31 (m, 24H), 0.90 (distorted t, *J* = 7.2 Hz, 12H); ^{13}C{^{1}H} NMR (75 MHz, $CDCl_3$): δ 146.5, 146.4, 135.1, 133.4, 133.0, 129.3, 128.3, 119.5, 119.5, 68.7, 48.9, 31.6, 31.4, 31.4, 31.1, 31.1, 28.9, 28.8, 22.6, 14.1; HRMS (ESI): *m*/*z* calcd. for $C_{48}H_{62}O_2S_4$ ([M + Na]$^+$) 821.3503, found 821.3539; m.p.: 146 °C.

Under an argon atmosphere, TFAA (2.8 ml, 33 mmol, 24 equiv) was added to a stirred solution of anhydrous DMSO (2.8 mL, 39 mmol, 48 equiv) in anhydrous CH_2Cl_2 (8.0 mL) at –60 ºC. After stirring at –60 ºC for 30 min, the diol obtained as above (0.65 g, 0.81 mmol) in CH_2Cl_2 (4.0 mL) was added. The reaction was stirred at –60 ºC for 1.5 h, and then triethylamine (8 mL, 57 mmol, 71 equiv) was added to the reaction. After stirring for 1 h, the reaction was allowed to warm up to room temperature and diluted with CH_2Cl_2. The organic phase was isolated and sequentially washed with 1 M HCl, water and brine, and then dried over Na_2SO_4, filtrated, and evaporated. The residue was purified by flash silica gel column chromatography (hexanes/CH_2Cl_2, 1:1). The isolated product was further purified by recrystallization from hot hexanes to give an orange solid (0.18 g, 0.23 mmol, 28%). ^{1}H NMR (300 MHz, $CDCl_3$): δ 7.34 (s, 4H), 5.50 (s, 2H), 2.99 (t, *J* = 7.6 Hz, 8H), 1.80 (quint, *J* = 7.5 Hz, 8H), 1.42–1.32 (m, 24H), 0.90 (distorted t, *J* = 7.1 Hz, 12H); ^{13}C NMR (75 MHz, $CDCl_3$): δ 180.8, 148.4, 135.8, 133.4, 124.5, 119.8, 56.3, 31.6, 31.4, 31.1, 28.8, 22.6, 14.1; HRMS (ESI): *m*/*z* calcd. for $C_{48}H_{58}O_2S_4$ ([M + Na]$^+$) 817.3217, found 817.3221; FT-IR (ATR): $\bar{\nu}_{max}$ (cm^{-1}) 2955, 2927, 2855, 1730, 1538, 1464, 1380, 826.

2,5-Bis(5-hexylthiophen-2-yl)-1,4-bis(trimethylsilylethynyl)benzene (5). A solution of 2-tributylstannyl-5-hexylthiophene (15 g, 33 mmol, 2.7 equiv), 1,4-dibromo-2,5-diiodobenzene (6.0 g, 12 mmol), and $Pd(PPh_3)_4$ (1.4 g, 1.2 mmol, 10 mol%) in dry DMF (30 mL) under an argon atmosphere was stirred at 80 °C for 3 days, then allowed to cool to room temperature. The mixture was partitioned between diethyl ether and water. The organic phase was isolated and the aqueous phase was extracted with diethyl ether. The combined organic phases were washed with brine, dried over Na_2SO_4, filtered, and evaporated. The resulting crude product was purified by flash column chromatography on silica gel containing 10 wt.% of anhydrous K_2CO_3 (CH_2Cl_2/hexanes, 1:2) to give 2,5-dibromo-1,4-bis(5-hexyl-2-thienyl)benzene as a colorless oil (5.7 g, 10 mmol, 81%). ^{1}H NMR (300 MHz, $CDCl_3$): δ 7.76 (s, 2H), 7.18 (d, *J* = 3.7 Hz, 2H), 6.78 (d, *J* = 3.5 Hz, 2H), 2.84 (t, *J* = 7.5 Hz, 4H), 1.72 (quint, *J* = 7.5 Hz, 4H), 1.50–1.24 (m, 12H), 0.88 (distorted t, *J* = 6.8 Hz, 6H); ^{13}C NMR (100 MHz, $CDCl_3$): δ 148.0, 137.1, 135.8, 135.6, 128.2, 124.3, 120.9, 31.7, 30.2, 29.0, 22.7, 14.2; HRMS (EI): *m*/*z* calcd. for $C_{26}H_{32}Br_2S_2$ (M^+) 566.0312, found 566.0305.

To a solution of 2,5-dibromo-1,4-bis(5-hexyl-2-thienyl)-benzene (2.1 g, 3.7 mmol), $PdCl_2(PPh_3)_2$ (0.35 g, 0.50 mmol, 13 mol%) and CuI (0.20 g, 1.1 mmol, 28 mol%) in dry THF (70 mL) under an argon atmosphere were added *N*,*N*-diisopropylamine (7.5 mL, 54 mmol, 14 equiv) and trimethylsilylacetylene (2 mL, 14 mmol, 3.8 equiv) at room temperature. The resultant mixture was stirred at reflux for 2 days, and then allowed to cool to room temperature before treated with sat. NH_4Cl. The resulting mixture was extracted with dichloromethane. The combined organic phases were washed with brine, dried over Na_2SO_4, filtered, and evaporated. The crude product was purified by column chromatography on neutral activated alumina (hexanes) to give the target compound as a brown solid (1.7 g, 2.8 mmol, 76%). ^{1}H NMR (300 MHz, $CDCl_3$): δ 7.68 (s, 2H), 7.54 (d, *J* = 3.7 Hz, 2H), 6.75 (d, *J* = 3.5, 2H), 2.83 (t, *J* = 7.1 Hz, 4H), 1.71 (quint, *J* = 7.1 Hz, 4H), 1.42–1.27 (m, 12H), 0.90 (distorted t, *J* = 6.9 Hz, 6H), 0.26 (s, 18H); ^{13}C NMR (75 MHz, $CDCl_3$): δ 147.2, 138.1, 134.4, 134.0, 127.1, 124.5, 120.1, 104.7, 101.3, 31.7, 31.6, 30.3, 28.9, 22.6, 14.1, –0.4; HRMS (ESI): calcd. for $C_{36}H_{50}Si_2S_2$ ([M + Na]$^+$) 625.2790, found 625.2768.

2,8-Dihexylanthra[1,2-*b*:5,6-*b*']dithiophene (C_6-BADT). To a solution of **5** (1.8 g, 2.9 mmol) in dry THF (40 mL) was added dropwise a solution of tetrabutylammonium fluoride (1.0 M, 10 mL, 10 mmol, 3.4 equiv) at 0 °C, and the resulting solution was stirred at room temperature for 1 h. The solvent was then evaporated, and the crude product was purified by column chromatography on silica gel (hexanes) to give the desilylated intermediate as a yellow solid (0.98 g, 2.1 mmol, 72%). ^{1}H NMR (300 MHz, $CDCl_3$): δ 7.72 (s, 2H), 7.52 (d, *J* = 3.7 Hz, 2H), 6.77 (d, *J* = 3.7 Hz, 2H), 3.37 (s, 2H), 2.84 (t, *J* = 7.1 Hz, 4H), 1.76–1.66 (m, 4H), 1.41–1.28 (m, 12H), 0.90 (distorted t, *J* = 7.1 Hz, 6H); ^{13}C NMR (75 MHz, $CDCl_3$): δ 147.5, 137.7, 134.8, 127.3, 124.8, 119.7, 83.4, 83.0, 31.6, 30.2,

28.9, 22.6, 14.1; HRMS (MALDI-TOF): calcd. for $C_{30}H_{34}S_2$ (M^+) 458.2090, found 458.2096; m.p.: 66 °C.

$InCl_3 \cdot 4H_2O$ (41 mg, 0.14 mmol, 13 mol%) was dehydrated by heating in a Schlenk flask under vacuum, to which the intermediate obtained as above (0.50 g, 1.1 mmol) and xylenes (30 mL) were added under an argon atmosphere. The resultant mixture was stirred at 120 °C for 12 h and then allowed to cool to room temperature before filtrated through Celite. The filtrate was evaporated and the crude product was purified by flash silica gel column chromatography (CH_2Cl_2/hexanes, 1:4) to give **C_6-BADT** as a yellow solid (0.45 g, 0.98 mmol, 90%). The product was identified by comparing its ^{1}H NMR spectrum with the literature data.[28] ^{1}H NMR (300 MHz, $CDCl_3$): δ 8.59 (s, 2H), 7.85 (d, *J* = 7.9 Hz, 2H), 7.70 (d, *J* = 7.9 Hz, 2H), 7.16 (s, 2H), 3.01 (t, *J* = 7.5 Hz, 4H), 1.82 (quint, *J* = 7.3 Hz, 4H), 1.46–1.27 (m, 12H), 0.91 (distorted t, *J* = 7.0 Hz, 6H); m.p.: 111 °C (lit. 117–119).

2,8-Dihexyl-6,12,13,17-tetrahydro-6,12-[4,5]epidioxolo-anthra[1,2-*b*:5,6-*b′*]dithiophen-15-one (6). C_6-BADT (0.45 g, 0.98 mmol) and vinylene carbonate (2.5 mL, 39 mmol, 40 equiv) in anhydrous toluene (30 mL) were added to an autoclave and stirred at 180 ºC for 3 days. The reaction mixture was cooled to room temperature and the solvent was evaporated to afford an oil, which solidified by the addition of methanol (5 mL). After filtration, the crude product was purified by flash silica gel column chromatography (hexanes) to give the vinylene carbonate adduct as a pale yellow solid (0.41 g, 0.74 mmol, 76%). ^{1}H NMR (300 MHz, $CDCl_3$): δ 7.53 (d, *J* = 7.9 Hz, 1H), 7.52 (d, *J* = 7.9 Hz, 1H), 7.40 (d, *J* = 7.9 Hz, 2H), 7.01 (s, 1H), 6.99 (s, 1H), 5.03–4.98 (m, 4H), 2.93–2.86 (m, 4H), 1.75 (quint, *J* = 7.2 Hz, 4H), 1.47–1.26 (m, 12H), 0.89 (distorted t, *J* = 6.4 Hz, 6H); ^{13}C NMR (75 MHz, $CDCl_3$): δ 154.3, 147.5, 147.0, 140.6, 137.5, 136.5, 132.3, 132.2, 131.1, 130.7, 123.2, 122.2, 121.8, 121.7, 121.4, 121.3, 76.2, 46.5, 46.4, 31.6, 31.1, 31.1, 31.0, 28.9, 28.8, 22.6, 14.1; HRMS (ESI): *m*/*z* calcd. for $C_{33}H_{36}O_3S_2$ ([M + Na]$^+$) 567.2004, found 567.2004; m.p.: 83 °C.

2,8-Dihexyl-6,12-dihydro-6,12-ethanoanthra[1,2-*b*:5,6-*b′*]dithiophene-13,14-dione (2). To a solution of 4 M NaOH (15 mL) were added THF (30 mL) and compound **6** (0.32 g, 0.59 mmol) under a nitrogen atmosphere, and the mixture was stirred at reflux for 2 h. After cooling to room temperature, the mixture was neutralized with 1 M HCl. After the addition of water, the mixture was extracted with chloroform, and the combined organic layers were washed with brine, dried over Na_2SO_4, filtered, and evaporated. The crude product was purified by flash silica gel column chromatography (hexanes/EtOAc, 4:1) to give the corresponding diol as a pale yellow solid (0.21 g, 0.41 mmol, 69%). ^{1}H NMR (300 MHz, $CDCl_3$): δ 7.50 (d, *J* = 7.7 Hz, 1H), 7.45 (d, *J* = 7.9 Hz, 1H), 7.42 (d, *J* = 8.1 Hz, 1H), 7.36 (d, *J* = 7.9 Hz, 1H), 7.00 (s, 1H), 6.98 (s, 1H), 4.79 (d, *J* = 2.6 Hz, 1H), 4.74 (d, *J* = 2.6 Hz, 1H) 4.23–4.13 (m, 2H), 2.89 (t, *J* = 7.6 Hz, 4H), 2.16 (two overlapping d, 2H), 1.74 (quint, *J* = 7.7 Hz, 4H), 1.41-1.25 (m, 12H), 0.89 (distorted t, *J* = 7.0 Hz, 6H); ^{13}C NMR (75 MHz, $CDCl_3$): δ 146.6, 140.0, 138.0, 123.4, 121.6, 121.3, 121.2, 120.8, 120.7, 69.0, 68.0, 50.2, 49.9, 31.6, 31.2, 31.1, 31.0, 31.0, 28.9, 28.8, 22.6, 14.0; HRMS (ESI): *m*/*z* calcd. for $C_{32}H_{38}O_2S_2$ ([M + Na]$^+$) 541.2211, found 541.2220; m.p.: 136 °C.

TFAA (2.0 ml, 14 mmol, 18 equiv) was added to a stirred solution of DMSO (2.0 mL, 28 mmol, 36 equiv) in anhydrous CH_2Cl_2 (7.3 mL) at –60 ºC under an argon atmosphere. After stirring at the same temperature for 30 min, the diol obtained as described above (400 mg, 0.77 mmol) in CH_2Cl_2 (4.5 mL) was added to the reaction. The reaction was further stirred at –60 ºC for 1.5 h, and then triethylamine (5.5 mL, 39 mmol, 51 equiv) was added to the reaction. After stirring for 1 h, the reaction was allowed to warm up to room temperature, before diluted with CH_2Cl_2. The organic phase was washed sequentially with 1 M HCl, H_2O and brine, dried over Na_2SO_4, filtered, and evaporated. The crude product was purified by flash silica gel column chromatography (CH_2Cl_2). The isolated material was further purified by recrystallization from toluene and hexanes to give the pure target compound as an orange solid (0.23 g, 0.44 mmol, 57%). ^{1}H NMR (300 MHz, $CDCl_3$): δ 7.67 (d, *J* = 8.1 Hz, 2H), 7.47 (d, *J* = 8.1 Hz, 2H), 7.06 (s, 2H), 5.27 (s, 2H), 2.93 (t, *J* = 7.5 Hz, 4H), 1.76 (quint, *J* = 7.3 Hz, 4H), 1.42–1.28 (m, 12H), 0.89 (distorted t, *J* = 7.0 Hz, 6H); ^{13}C NMR (75 MHz, $CDCl_3$): δ 182.3, 148.4, 141.9, 137.0, 129.4, 129.2, 123.8, 122.6, 121.5, 58.1, 31.6, 31.1, 31.0, 28.8, 22.6, 14.1; HRMS (ESI): *m*/*z* calcd. for $C_{32}H_{34}O_2S_2$ ([M + Na]$^+$) 537.1898, found 537.1911; IR (ATR): $\bar{\nu}_{max}$ (cm^{-1}) 2953, 2926, 2855, 1748, 1732, 1466, 1444, 1407, 1114, 1048, 837, 725.

Single-crystal X-ray diffraction measurements. The crystallographic data of compound **C_6-ATT** were recorded on a Bruker-APEXII X-Ray diffractometer equipped with a large area CCD detector by using graphite monochromated Mo Kα radiation (λ = 0.71073 Å). The crystallographic data of compounds **1** and **2** were recorded on a Rigaku R-AXIS RAPID/S imaging plate diffractometer with graphite monochromated Mo Kα radiation. The structures were refined with the SHELXL-97. Crystallographic data for **C_6-ATT**: $C_{46}H_{58}S_4$, M_w = 739.16, monoclinic, space group $P2_1/n$ (No. 14), a = 12.604(2), b = 4.8761(9), c = 32.657(6) Å, β = 100.676(4)°, V = 1972.3(6) Å^3, ρ_{calcd} = 1.245 g cm^{-3}, T = 90(2) K, Z = 2, R_1 = 0.0574 [$I > 2.0\ \sigma(I)$], Rw = 0.1098 (all data), GOF = 1.013. Crystallographic data for **1**: $C_{48}H_{58}O_2S_4 \cdot 0.5(C_6H_{14})$, M_w = 838.27, triclinic, space group P-1 (No. 2), a = 10.9591(3), b = 11.8130(3), c = 19.6453(5) Å, α = 104.6590(10), β = 96.3200(10), γ = 103.8200(10)°, V = 2349.57(11) Å^3, ρ_{calcd} = 1.185 g cm^{-3}, T = 193(2) K, Z = 2, R_1 = 0.0605 [$I > 2.0\ \sigma(I)$], Rw = 0.1930 (all data), GOF = 1.102. Crystallographic data for **2**: $C_{32}H_{34}O_2S_2$, M_w = 514.74, monoclinic, space group $P2/c$ (No. 13), a = 12.4700(5), b = 13.7514(5), c = 16.2964(6) Å, β = 105.0607(8)°, V = 2698.51(16) Å^3, ρ_{calcd} = 1.267 g cm^{-3}, T = 103(2) K, Z = 4, R_1 = 0.0589 [$I > 2.0\ \sigma(I)$], Rw = 0.1559 (all data), GOF = 1.050. CCDC-1052010 (**C_6-ATT**), CCDC-1052256 (**1**), and CCDC-1052257 (**2**) contain the supplementary crystallographic data for this paper.

4.2. Photoreaction quantum yield determination

A chemical actinometer ($K_3[Fe(C_2O_4)_3]$)[36] was used for quantum yield determination of the photochemical reaction of **ADK** in toluene. A square quartz cuvette (10 mm I.D.) that contained a deaerated solution (3.0 ml) of **ADK** was irradiated with 468-nm light through a monochromator (Ritsu MC-10N) by using a 500-W xenon lamp (Ushio XB-50102AA-A). The photochemical reaction was monitored by using a JASCO UV/Vis/NIR V-570 spectrophotometer. The quantum yields were determined from the increase in absorbance of anthracene at 378 nm in the beginning of the reaction. The Φ_r values of other compounds (**TDK**, **PDK**, **1**, and **2**) were measured by the relative method using the value for **ADK** (Φ_r = 0.37) as the standard.

4.3. Film preparation and characterization

Three methods were employed to prepare the films of **C_6-ATT** and **C_6-BADT**: (a) Vacuum deposition of **C_6-ATT** or **C_6-BADT** with a deposition rate of 1.8 nm min^{-1}; (b) The photoprecursor approach in which a solution of **1** or **2** in chloroform (10 mg mL^{-1}) was spin-coated at 800 rpm for 30 s and the resulting film was irradiated with a blue LED ($\lambda \approx 470$ nm) at 200 mW cm^{-2} for 30 min in a nitrogen-filled glovebox; (c) Direct spin coating of a solution of **C_6-ATT** or **C_6-BADT** in chlorobenzene/chloroform (1:1 by volume, 10 mg mL^{-1}) at 800 rpm for 30 s. The thicknesses of the resulting films were measured by Bruker DektakXT. UV–vis absorption spectra of thin films on glass substrates were recorded in air using a JASCO V-650 spectrometer. Ionization energies were measured on a Bunko Keiki AC-3 photoelectron spectroscopy instrument. The surface morphology of organic films was observed by an SII SPA400/SPI3800N atomic force microscope (AFM) in tapping mode using a silicon probe with a resonant frequency of 138 kHz and a force constant of 16 N m^{-1} (SII, SI-DF20). The bulk structure of thin-films was evaluated by out-of-plane X-ray diffraction (XRD) measurements using a Rigaku SmartLab diffractometer equipped with a rotating anode (Cu Kα radiation, λ = 1.5418 Å). Hole mobility characteristics were measured by the space-charge-limited-current (SCLC) method using an Agilent Technologies 4155C Semiconductor Parameter Analyzer operated by Interactive Characterization Software (ICS), version 3.6.0.

Acknowledgement

This work was partly supported by Grants-in-Aid for Scientific Research (KAKENHI) Nos. 23685030, 25107519 ('AnApple'), 25288092, 25288113, 25620061, 26105004, 26288038, 26600004, and 26620167 from the Japan Society for the Promotion of Science (JSPS), the Murata Science Foundation, the PRESTO program by Japan Science and Technology Agency (JST), Leading Industrial Technology Creation Project by New Energy and Industrial Technology Development Organization (NEDO), and the program for promoting the enhancement of research universities in NAIST supported by the Ministry of Education, Culture, Sports, Science and Technology (MEXT). C.Q. thanks the JSPS for a post-doctoral fellowship. We thank Ms. Y. Nishikawa and Mr. Shohei Katao (NAIST) for help in mass spectrometry measurements and single-crystal X-ray diffraction analyses, respectively.

Notes and references

[a] Graduate School of Materials Science, Nara Institute of Science and Technology (NAIST), 8916-5 Takayama-cho, Ikoma, Nara 630-0192, Japan

[b] Dojindo Laboratories, 2025-5 Tabaru, Mashiki-machi, Kumamoto 861-2202, Japan

[c] Department of Organic Device Engineering, Yamagata University, 4-3-16 Jonan, Yonezawa, Yamagata 992-8510, Japan

[d] Core Research for Evolutional Science and Technology (CREST), Japan Science and Technology Agency (JST), 4-1-8 Honcho, Kawaguchi, Saitama 332-0012, Japan

† Electronic Supplementary Information (ESI) available: Photoreactions in solution, photoelectron spectroscopy in air, cyclic voltammetry, DFT calculations, simulated powder X-ray diffraction parameters, space-charge-limited-current measurements, NMR spectra of photoprecursors **1** and **2**. See DOI: 10.1039/b000000x/

1 C. Sekine, Y. Tsubata, T. Yamada, M. Kitano and S. Doi, *Sci. Technol. Adv. Mater.*, 2014, **15**, 034203.
2 B. Kang, W. H. Lee and K. Cho, *ACS Appl. Mater. Interfaces*, 2013, **5**, 2302–2315.
3 C. L. Chochos, N. Tagmatarchis and V. G. Gregoriou, *RSC Adv.*, 2013, **3**, 7160–7181.
4 P. F. Moonen, I. Yakimets and J. Huskens, *Adv. Mater.*, 2012, **24**, 5526–5541.
5 S. Kola, J. Sinha and H. E. Katz, *J. Polym. Sci. Part B Polym. Phys.*, 2012, **50**, 1090–1120.
6 X.-H. Zhu, J. Peng, Y. Cao and J. Roncali, *Chem. Soc. Rev.*, 2011, **40**, 3509–3524.
7 C. Zhong, C. Duan, F. Huang, H. Wu and Y. Cao, *Chem. Mater.*, 2011, **23**, 326–340.
8 A. Facchetti, *Chem. Mater.*, 2011, **23**, 733–758.
9 M. Watanabe, K.-Y. Chen, Y. J. Chang and T. J. Chow, *Acc. Chem. Res.*, 2013, **46**, 1606–1615.
10 S.-D. Jeong, B. Min, S. Y. Cho, C. Lee, B. K. Park, K.-S. An and J. Lim, *J. Org. Chem.*, 2012, **77**, 8329–8331.
11 T. Okujima, Y. Hashimoto, G. Jin, H. Yamada, H. Uno and N. Ono, *Tetrahedron*, 2008, **64**, 2405–2411.
12 S. Aramaki, Y. Sakai and N. Ono, *Appl. Phys. Lett.*, 2004, **84**, 2085–2087.
13 H. Uno, T. Ishikawa, T. Hoshi and N. Ono, *Tetrahedron Lett.*, 2003, **44**, 5163–5165.
14 S. Ito, T. Murashima, N. Ono and H. Uno, *Chem. Commun.*, 1998, 1661–1662.
15 One of the few exceptions is the use of benzoporphyrin in solution-processed photovoltaic active layers by employing its soluble precursor. Y. Matsuo, Y. Sato, T. Niinomi, I. Soga, H. Tanaka and E. Nakamura, *J. Am. Chem. Soc.*, 2009, **131**, 16048–16050.
16 M. Suzuki, T. Aotake, Y. Yamaguchi, N. Noguchi, H. Nakano, K. Nakayama and H. Yamada, *J. Photochem. Photobiol. C Photochem. Rev.*, 2014, **18**, 50–70.
17 Y. Yamaguchi, M. Suzuki, T. Motoyama, S. Sugii, C. Katagiri, K. Takahira, S. Ikeda, H. Yamada and K. Nakayama, *Sci. Rep.*, 2014, **4**.
18 H. Yamada, Y. Yamaguchi, R. Katoh, T. Motoyama, T. Aotake, D. Kuzuhara, M. Suzuki, T. Okujima, H. Uno, N. Aratani and K. Nakayama, *Chem. Commun.*, 2013, **49**, 11638–11640.
19 K. Nakayama, C. Ohashi, Y. Oikawa, T. Motoyama and H. Yamada, *J. Mater. Chem. C*, 2013, **1**, 6244–6251.

20 T. Motoyama, T. Kiyota, H. Yamada and K. Nakayama, *Sol. Energy Mater. Sol. Cells*, 2013, **114**, 156–160.
21 H. Yamada, C. Ohashi, T. Aotake, S. Katsuta, Y. Honsho, H. Kawano, T. Okujima, H. Uno, N. Ono, S. Seki and K. Nakayama, *Chem. Commun.*, 2012, **48**, 11136–11138.
22 A. A. Leitch, K. A. Stobo, B. Hussain, M. Ghoussoub, S. Ebrahimi-Takalloo, P. Servati, I. Korobkov and J. L. Brusso, *Eur. J. Org. Chem.*, 2013, **2013**, 5854–5863.
23 C. Fu, F. Rosei and D. F. Perepichka, *ACS Nano*, 2012, **6**, 7973–7980.
24 J. L. Brusso, O. D. Hirst, A. Dadvand, S. Ganesan, F. Cicoira, C. M. Robertson, R. T. Oakley, F. Rosei and D. F. Perepichka, *Chem. Mater.*, 2008, **20**, 2484–2494.
25 W.-J. Liu, Y. Zhou, Y. Ma, Y. Cao, J. Wang and J. Pei, *Org. Lett.*, 2007, **9**, 4187–4190.
26 Y. Yi, L. Zhu and J.-L. Brédas, *J. Phys. Chem. C*, 2012, **116**, 5215–5224.
27 A. Pietrangelo, B. O. Patrick, M. J. MacLachlan and M. O. Wolf, *J. Org. Chem.*, 2009, **74**, 4918–4926.
28 A. Pietrangelo, M. J. MacLachlan, M. O. Wolf and B. O. Patrick, *Org. Lett.*, 2007, **9**, 3571–3573.
29 F. He, W. Wang, W. Chen, T. Xu, S. B. Darling, J. Strzalka, Y. Liu and L. Yu, *J. Am. Chem. Soc.*, 2011, **133**, 3284–3287.
30 Y. Zhou, W.-J. Liu, W. Zhang, X.-Y. Cao, Q.-F. Zhou, Y. Ma and J. Pei, *J. Org. Chem.*, 2006, **71**, 6822–6828.
31 V. Mamane, P. Hannen and A. Fürstner, *Chem. – Eur. J.*, 2004, **10**, 4556–4575.
32 S. Masuo, K. Tanaka, M. Oe and H. Yamada, *Phys. Chem. Chem. Phys.*, 2014, **16**, 13483–13488.
33 S. Katsuta, H. Saeki, K. Tanaka, Y. Murai, D. Kuzuhara, M. Misaki, N. Aratani, S. Masuo, Y. Ueda and H. Yamada, *J. Mater. Chem. C*, 2014, **2**, 986–993.
34 M. Kochi, Y. Harada, T. Hirooka and H. Inokuchi, *Bull. Chem. Soc. Jpn.*, 1970, **43**, 2690–2702.
35 Y. Liu, M. s. Liu and A. k.-Y. Jen, *Acta Polym.*, 1999, **50**, 105–108.
36 C. G. Hatchard and C. A. Parker, *Proc. R. Soc. London, Ser. A*, 1956, **235**, 518–536.